Carbohydrate Polymers 230 (2020) 115571

Contents lists available at ScienceDirect

Carbohydrate Polymers

journal homepage: www.elsevier.com/locate/carbpol

A promising process to modify cellulose nanofibers for carbon dioxide (CO_2) adsorption

Sima Sepahvand[a], Mehdi Jonoobi[a,*], Alireza Ashori[b,*], Florent Gauvin[c], H.J.H Brouwers[c], Kristiina Oksman[d], Qingliang Yu[c,*]

[a] Department of Wood and Paper Science and Technology, Natural Resources Faculty, University of Tehran, Karaj, Iran
[b] Department of Chemical Technologies, Iranian Research Organization for Science and Technology (IROST), Tehran, Iran
[c] Department of the Built Environment, Eindhoven University of Technology P.O. Box 513, 5600 MB, Eindhoven, the Netherlands
[d] Division of Materials Science, Luleå University of Technology, 971 87, Luleå, Sweden

ARTICLE INFO

Keywords:
CO_2 adsorption
Cellulose nanofiber
Aerogels
Chemical modification

ABSTRACT

A novel process of using phthalimide to modify cellulose nanofibers (CNF) for CO_2 adsorption was studied. The effectiveness of the modification was confirmed by ATR-IR. Phthalimide incorporation onto CNF was confirmed with the characteristic peaks of NH_2, C–N, and ester bonding COO^- was observable. The XPS analyses confirmed the presence of N1s peak in Ph-CNF, meaning that the hydroxyl groups reacted with the amino groups (NH_2) of phthalimide on the CNF surface. Based on the results, surface modification and addition of phthalimide increased the specific surface area, but also decreased the overall porosity, size of pores and volume of pores. When the temperature, humidity, pressure, and airflow rate increased, the CO_2 adsorption significantly increased. The CO_2 adsorption of phthalimide-modified CNF was confirmed by ATR-IR spectroscopy as the characteristic peaks of HCO_3^-, NH_3^+ and ester bonding $NCOO^-$ were visible on the spectra.

1. Introduction

A continuous increment in atmospheric carbon dioxide (CO_2) concentration, the second-largest greenhouse effect after water, has attracted significant attention worldwide (Dassanayake, Gunathilake, Jackson, Jaroniec, & Abidi, 2016). CO_2 is responsible for more than 75% of total greenhouse gases emissions (Ansaloni, Salas-Gay, Ligi, & Baschetti, 2017), and it is widely known that the increase in CO_2 concentration in the atmosphere is a major reason for global warming. A recent study claimed that CO_2 concentration of CO_2 in the air has increased from approximately 270 ppm before the industrial revolution to near 400 ppm today (Darunte, Walton, Sholl, & Jones, 2016). The continued emission and accelerated increase of concentration in the atmosphere has led to an increased need for efficient, low-cost technologies/devices to capture CO_2 (Hornbostel et al., 2013). Many technologies applying various materials that involve different adsorption mechanisms have been developed for CO_2 capture. Among these, absorption processes based on alkanol-amine-water solutions are widely used (Aaron & Tsouris, 2005) because amines react selectively with atmospheric CO_2 in the presence of moisture at suitable temperature and pressure (Choi, Drese, Eisenberger, & Jones, 2011). In particular, some porous organic polymers have attracted great attention because of their high surface area, low density, and excellent thermal, chemical, and water stabilities (Sung & Suh, 2014). Conventional fibrous media usually suffers from many structural and performance drawbacks such as large fiber diameter, non-uniform fiber diameter and size of pores, relatively low filtration efficiency, high basis weight, and poor high temperature resistance (Adiletta, 1999). It has been well documented that the smaller the fiber diameter, the better the filtration performance and efficiency. Hence, nanofibers could provide high-efficiency filtration by offering a superior “slip effect” that would cause less resistance against the flow, leading to a smaller pressure drop across the fibrous media (Hung & Leung, 2011; Yoon, Hsiao, & Chu, 2008; Ma, Hsiao, & Chu, 2011). Due to its importance, monitoring of CO_2 concentration is inevitable, and air purification filters are the most important tool to achieve this task (Mahfoudhi & Boufi, 2017). There are two main types of air filters, namely particulate air filters and chemical air filters. The porous fibrous membranes that make up air filters clean only solid particle pollutants (Liu et al., 2017).

Typically, there are certain requirements for materials that are used for the adsorption of pollutants: (1) low cost, (2) good mechanical and structural integrity to overcome air flow for a specific amount of time, (3) high adsorption capacities with high rates, and (4) a cost-effective regeneration capacity (Mahfoudhi & Boufi, 2017). Among these

* Corresponding authors.
E-mail addresses: mehdi.jonoobi@ut.ac.ir (M. Jonoobi), ashori@irost.ir (A. Ashori), q.yu@bwk.tue.nl (Q. Yu).

https://doi.org/10.1016/j.carbpol.2019.115571
Received 10 August 2019; Received in revised form 31 October 2019; Accepted 4 November 2019
Available online 06 November 2019
0144-8617/

materials, activated carbons have a variety of advantages such as low cost, large pore volume, easy-to-design pore structure, hydrophobicity, high thermal stability, and low energy consumption for regeneration (Hao, Li, & Lu, 2011; Jonoobi, Ashori, & Siracusa, 2019; Stein, Wang, & Fierke, 2009). However, most activated carbons exhibit a relatively low CO_2 adsorption capacity (typically between 2 and 3 mmol.g^{-1} under 25 ℃, 1 atm) (Fan, Zhang, Zhang, Shu, & Shi, 2013). However, recent studies have shown that nano cellulose, specially functionalized nanofibrillated cellulose (CNF) with amine and aminosilane, has a good capability for CO_2 sorption (Gebald, Wurzbacher, Borgschulte, Zimmermann, & Steinfeld, 2014; Sehaqui et al., 2015). CNF is a unique material with outstanding features such as large aspect ratios, great specific surface area, excellent biodegradability, high strong mechanical properties, eco-friendliness, decomposable property, non-toxicity, light weight, obtainability from different biobased sources/residual, and chemical modification capability due to abundant hydroxyl groups (Chaabouni & Boufi, 2017; Khanjanzadeh et al., 2019). Generally, amine-based derivatives are among the most prevalent groups used to boost adsorption capacity (Mahfoudhi & Boufi, 2017). These groups could be introduced into nanocellulose in two different ways: as part of the process to prepare the nanocellulose or by altering of the nanofibers surface (Mahfoudhi & Boufi, 2017). In addition to physical properties (such as specific surface area, size of pore and volume of pores), chemical composition could significantly affect CO_2 adsorption, e.g., heteroatom ring nitrogen and groups having a strong affinity towards CO_2 like COO, C═O, OH, and NH_2 (Dawson, Adams, & Cooper, 2011). The main goal of this research was to investigate the CO_2 adsorption of porous CNF as a sustainable renewable material, modified using phthalimide (1,3-dihydro-1,3-dioxoisoindole;) for reactive amino groups. In general, the hydrogen bonding ability of the amide connection causes strong interaction; so, phthalimide is expected to have the potential to be a good choice for CO_2 adsorption, as phthalomide has C═O, COO, and the NH_2 appeared in it after opening the ring (Sepahvand et al., 2019). There is a lack of research on the utilization of phthalimide as a coupling agent modifier for CNF in the production of an adsorbent, especially considering CO_2 adsorption. To the best of our knowledge, this is the first attempt to utilize a CNF modified with amino-based phthalimide for CO_2 adsorption.

2. Materials and methods

2.1. Materials

Birch Kraft pulp, kindly provided by SCA Munksund AB (Piteå, Sweden), was ground as the raw material in an ultrafine friction grinder MKZA10-20 J (Masuko Sangyo Co., Japan) at 2 wt % consistency for the CNF fibrillation process. Prior to the grinding process, the suspension was dispersed using a shear mixer (Silverson L4RT Silverson Machine Ltd., England). The grinding stones were set to contact mode after the initial feeding of the suspension and gradually adjusted until reaching 90 μm (negative). The stones were coarse silicon carbide (SiC) and the rotor speed was set to 1500 rpm. The grinding was stopped after gel with the maximum viscosity was reached (Jonoobi, Harun, Mathew, & Oksman, 2010).

The phthalimide (1, 3-dihydro-1, 3- dioxisoindole; $C_6H_4(CO)_2NH$) was supplied by Merck (Germany) and the acetic acid (99.5%, purity) used to resolve the phthalimide was supplied by Sigma Aldrich (USA).

2.2. Chemical modification

Phthalimide powder was added to a mixture of water/acetic acid (96/4 (v/v)) with a ratio of 0.5, 1.0, and 1.5 wt %. Since phthalimide is sensitive to direct heat, it was placed inside glycerol oil and continuously stirred at 80 °C for 24 h. The CNF gel was prepared with a concentration of 1 wt % and stirred at 480 rpm for 3 h at room temperature. Subsequently, phthalimide was added to the CNF gel and stirred at 65 °C for 3 h. The pH of the solution was set at 4 by using Ca $(OH)_2$. The solution of the CNF-phthalimide was centrifuged at 2500 rpm for 10 min to remove the extra phthalimide which did not react with the CNF. A Teflon mold (with a 30 mm diameter and 40 mm length) was mounted on a cylindrical metal base of copper with a 100 mm height and 40 mm diameter. The diluted solution was poured into the Teflon mold in order to create a homogeneous structure, prevent crack and fracture of samples during freezing and the bottom 30 mm of the mold was then placed in liquid N_2 at a temperature of −196 °C. In the last step, the mixture was poured in the copper cylinder and then immersed in liquid N_2 at a temperature of −196 °C. The frozen sample was dried in a freeze dryer (Alpha 1–4 LD plus from Martin Christ) under the following conditions: ice condenser = −57 °C; vacuum ≤ 0.1 mbar; and time = 48 h. The resulting materials are referred to as 0.5% phthalimide-CNF, 1% phthalimide-CNF, and 1.5% phthalimide-CNF; unmodified CNF was used as a control sample.

2.3. Characterizations

2.3.1. (XPS) analysis

In order to investigate the surface modification of CNF aerogels, the x-ray photoelectron spectroscopy (XPS) was used. The XPS analyses were conducted by using a ThermoScientificK-Alpha spectrometer (UK) which was fitted out with a monochromatic small-spot x-ray source and a 180° double-focusing hemispherical analyzer with a 128 channel detector. The spectra were obtained using an aluminum anode (Al Kα = 1486.6 eV) operating at 72 W with a spot size of 400 μm. Survey scans and region scans were measured at 200 eV and 50 eV, respectively.

2.3.2. Transmission electron microscopy (TEM)

Aqueous suspensions (0.1 w/w %) of both CNF and CNF-Ph were prepared for TEM analysis. The samples were 100 x diluted in water. A drop (10 μL) of aqueous suspension was deposited on a 200 mesh Cu grid covered with a continuous carbon film. The morphology of CNF and CNF-Ph was observed using a FEI Tecnai 20 Sphera (Company FEI, Eindhoven, Netherlands) instrument with a LaB6 filament, operated at an accelerating voltage of 200 kV.

2.3.3. Scanning electron microscopy (SEM)

The morphology of the modified and unmodified CNF aerogels was observed after CO_2 adsorption using an SEM with the BSE detector (Phenom ProX, Eindhoven, Netherlands) at an accelerating voltage of 10 kV. All samples were sputter-coated (2 min and 25 mA) with a gold layer of approximately 15 nm in thickness.

2.3.4. Density and porosity

The apparent densities of Ph-CNF (ρ_a) were calculated by measuring the mass and volume of each aerogel. The weight of the aerogel was measured using analytical balance (readability 0.0001 g, Analytical Balance, Mettler Toledo, USA) and the dimensions (diameter and height) of the aerogel were measured using a digital caliper at four different positions. The aerogel porosity (P) was determined by the density of the aerogel (ρ_a) and the density of CNF (ρ_C) according to the following equation:

$$P\% = \left(1 - \frac{p_a}{p_c}\right) \times 100 \quad (1)$$

2.3.5. BET specific surface area and pore size distribution

The Brunauer-Emmett-Teller specific surface area (BET) of the prepared aerogels was determined by N_2 physisorption using TriStar II Micromeritics (Instrument Corp., USA). Aerogel samples (0.1-0.2 g) were first dried at 115 °C for 4 h and then degassed at 115 °C for 18 h prior to the analysis. The analysis was followed by N_2 adsorption at

−196 °C. BET analysis was carried out for a relative vapor pressure (P/P_0) of 0.01-0.3 at −196 °C. The average size of pores of the CNF and Ph-CNF aerogels was estimated from the nitrogen desorption isotherm according to Barrett-Joyner-Halender (BJH) analysis. In addition, the volume of pores (VP) was determined by the density of the aerogel (ρ_a) according to the following equation:

$$VP = \frac{1}{\rho_a} - \frac{1}{1.5} \quad (2)$$

2.3.6. Infrared spectroscopy (ATR-IR)

The CNF and Ph-CNF aerogels with phthalimide were analyzed with a Perkin Elmer Frontier™ Spectrometer (spectrum 400 FT-IR, USA) using the attenuated total reflection (ATR) method (GladiATR) to see if grafting occurred. Spectra were obtained by measuring the 400–4000 cm^{-1} range at a resolution of 4 cm^{-1}.

2.3.7. CO_2 adsorption

Pressurized air with a CO_2 concentration of 500 ppm was used to evaluate the adsorption capacity of the CNF aerogel. CO_2 adsorption analysis were conducted at different air flow rates (0, 0.2, 0.4, 0.6, and 0.8 L/min), pressures (0, 0.2, 0.4, 0.8, as well as 1 bar), temperatures (0, 25, 45, 65, and 85°C), and relative humidity's (0, 25, 40, 65, 80, and 95%) at a constant time of 8 h. The CO_2 adsorption efficiency (η) was experimentally calculated from the CO_2 concentration. Steady state was achieved according to the expression given by Eq. (3) (Molina & Bouallou, 2016).

$$\eta = \frac{C_{CO_2in} - C_{CO_2out}}{C_{CO_2in}} \times 100 \quad (3)$$

where C_{co_2in} and $C_{co_2out}$are the inlet and outlet CO_2 concentration, respectively. Outlet CO_2 concentration is a phenomenon whereby CO_2 passes through the surface.

2.3.8. Air flow permeability (pressure drop, ΔP) and quality factor (QF) measurement

The permeability of the adsorbent is defined as the quantity of air which goes through the sample surface during an assured time (1 s) at the surface established conditions of the test and pressure drop. The cylindrical aerogel sample composition for all the test filters was similar with effective diameter (28 mm) and height (12 mm), which was the thickness equivalent of the filter. The suction flow was provided by a vacuum pump and increased progressively till a stable depression of 100 Pa was reached. The aerogel permeability was obtained by dividing the airflow rate by the effective aerogel area, according to Eq. (4) (Olmedo, Aragón, Garcia, Torrent, & Ramón, 2008).

$$R = \frac{Q/T}{A}\left(\frac{ml/s}{cm^2}\right) \quad (4)$$

The permeability (R) was based on the flow of gas (Q) at time (T) and the specific pressure of the cross-section of the filter (A). The performance of porous filters is typically shown with a quality factor (QF), also known as the figure of merit, which is the ratio of the penetration rate of articles η to the pressure drop across the filter ΔP, QF was calculated according to Eq. (5) (Shou et al., 2015).

$$QF = -Ln(1 - \eta\%)/\Delta P \quad 5)$$

where QF is the quality factor, η is the CO_2 adsorption efficiency, and ΔP is the pressure drop.

2.4. Statistical analysis

All the data were subjected to Analysis of Variance (ANOVA) and the difference between means was evaluated using Duncan's Multiple Range Test at a confidence level is 95%. The SPSS statistic program (Version 20.0) was used for data analysis.

3. Results and discussion

3.1. X-ray photoelectron spectroscopy (XPS)

The XPS spectra of the CNF and Ph-CNF aerogels are shown in Fig. 1(A–C). Fig. 1(A) shows the spectrum of CNF and surface Ph-CNF. As expected, the spectrum of CNF only shows two peaks in the range of 284.7 eV and 536.34 eV, which are related to carbon (C1s) and oxygen (O1s), respectively. On the other hand, besides the oxygen and carbon peaks, new nitrogen (N1s)-related peak in the range of 399.36 eV appears for the Ph-CNF (Lu, Askeland, & Drzal, 2008). As Fig. 1(B) shows, the spectrum of nitrogen (N1s region) is fitted with two peaks. The peak at 399.36 eV can be attributed to the presence of free amino groups ($-NH_2$) in the phthalimide after opening the ring. The formation of an amine group confirms the presence of amino groups on the surface of

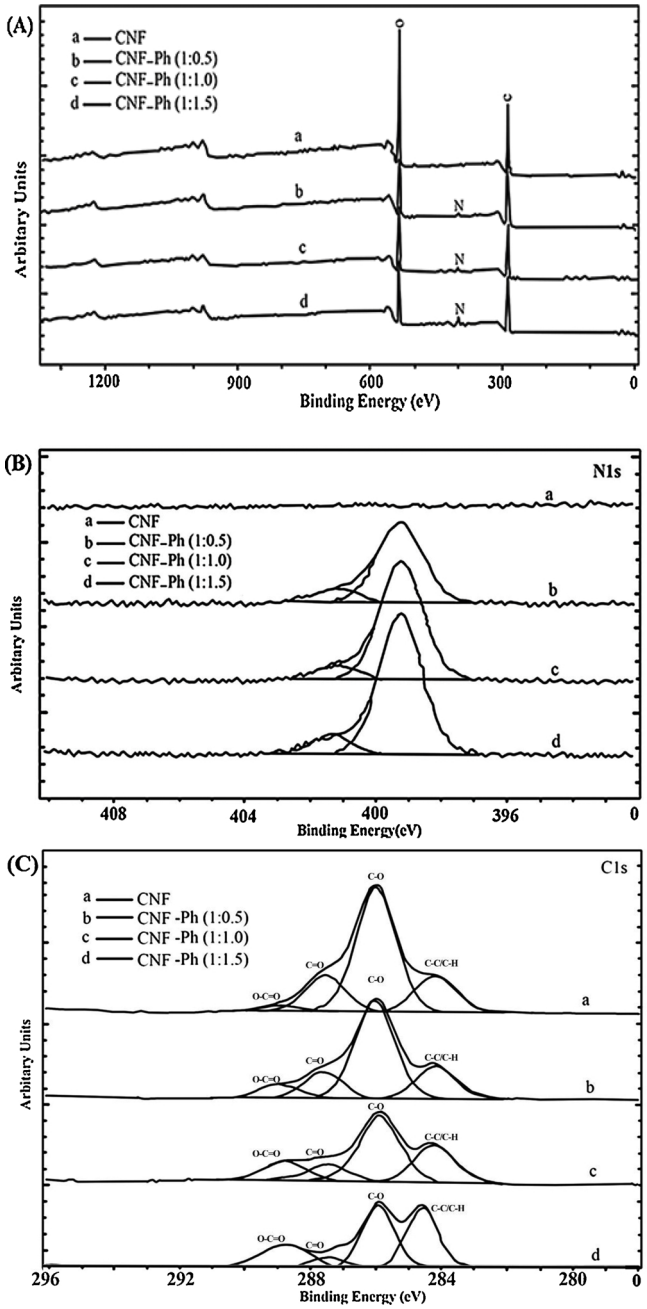

Fig. 1. XPS spectrum of CNF and Ph-CNF (A), deconvolution of its N_{1s} peak (B), and deconvolution of its C_{1s} peak (C).

Table 1
Atomic surface concentration (at %) of CNF and Ph-CNF aerogels.

	O/C	C_{1s}	O_{1s}	N_{1s}
CNF	0.75	58.60	44.09	–
CNF-Ph0.5	0.67	61.02	40.73	1.2
CNF-Ph1.0	0.48	62.82	30.26	3.7
CNF-Ph1.5	0.42	66.00	27.50	4.2

the CNF (Böcking, James, Coster, Chilcott, & Barrow, 2004; Lu et al., 2008). This peak's intensity increases with increased phthalimide loading. Moreover, the peak at 401.4 eV is related to quaternary type nitrogen functionalities (Song & Peng, 2009). Fig. 1(C) shows the C1s spectrum for CNF and Ph-CNF. In this spectrum the presence of four types of carbon bonds are observed, these bonds correspond to the following carbon interactions for CNF: C1 (C−C/C–OH) 284.7 eV, C2 (C–O, C–N) 286.4 eV, C3 (C═O, N−C═O) 287.6 eV, and C4 (O−C═O) 289.2 eV (Gao et al., 2013), also for Ph-CNF C1 (C−C/C–OH) 284.5 eV, C2 (C–O, C–N) 286.1 eV, C3 (C═O, N−C═O) 288 eV, and C4 (O−C═O) 289 eV. Pure CNF shows only a negligible amount of the carboxylic group (O−C═O), but after modification with phthalimide it can be observed that the intensity of the C1 and C4 peaks increases while the intensity of the C2 and C3 peaks decreases. The C1s spectrum for pure phthalimide consists of two main peaks: The first peak at the higher binding energy (289.3 eV) corresponds to C═O atoms while the second peak is attributed to the phenylene ring (C–H) at the binding energy of 286 eV (Chenite & Selmani, 1994). The relative atomic concentration and oxygen-to-carbon (O/C) ratios are summarized in Table 1. Marginally below the 0.83 value of theoretical O/C, XPS measurement gives the O/C atomic ratio of CNF of 0.75. This is possibly due to the existence of pollutants and other compounds on the surface (Tingaut, Hauert, & Zimmermann, 2011). Furthermore, the O/C ratio decreases when the amount of phthalimide (0.5, 1 and 1.5%) increases from 0.75 to 0.67, 0.48, and 0.42, respectively. The reduction in the O/C, the presence of the NH_2 group in the Ns1 spectra, and the corresponding increase in the contribution of the C1 and C4 carbons (C−C/C–OH and O−C═O) clearly show the occurrence of expected surface modification of the CNF.

3.2. Morphology analysis

3.2.1. TEM

The structure and size of the CNF were studied by transmission electron microscopy (TEM). Fig. 2A shows the TEM image of the isolated CNF, indicating that the used CNF are below 100 nm, the diameter ranged from 20 to 50 nm, and the length is estimated to be several micrometers. It should be noted that the surface charge of CNF, measured by zeta potential, was -52.5 (Sepahvand et al., 2019).

3.2.2. SEM before and after of CO_2 adsorption

The morphology of the modified CNF before and after CO_2 adsorption tests were examined by SEM and is shown in Fig. 2B (a and b), respectively. Fig. 2B (a) indicates that the modified CNF aerogel morphology has a sheet-forming structure due to the existence of phthalimide in the surface CNF; also, as can be seen, the surface consists of many pores resulting in high porosity. Fig. 2B (b) illustrates that there is no change in the structure of the modified CNF, even in the volume of pores or porosity, after the adsorption of CO_2, which was confirmed by the BET test. This is owing to the presence of amine groups on the surface CNF, which can react with CO_2 without making any changes on the surface. Indeed, it seems that the CO_2 adsorption occurs on the surface (Gebald, Wurzbacher, Tingaut, Zimmermann, & Steinfeld, 2011).

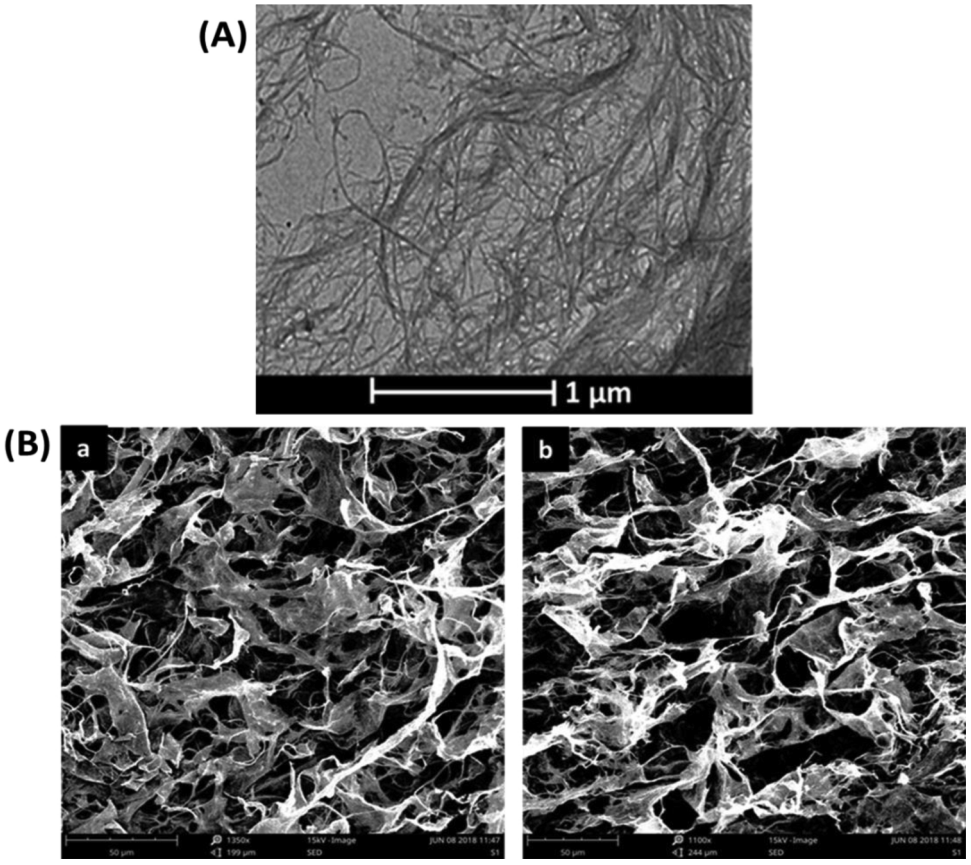

Fig. 2. A) TEM image of CNF. B) SEM of CNF and phthalimide-modified CNF (a) before and (b) after CO_2 adsorption test.

Table 2
BET surface area, size of pores and volume of pores CNF and Ph-CNF aerogels.

Sample	Density (g/cm^3)	BET (m^2/g)	Aver. size of pores (nm)	Porosity (%)	volume of pores (cm^3/g)
CNF	0.0105^{a*}	272^{a}	14.3^{a}	99.4^{a}	94.6^{a}
CNF-Ph0.5	0.0112^{a}	283^{b}	11.5^{b}	99.2^{a}	88.6^{b}
CNF-Ph1.0	0.0138^{b}	319^{c}	7.4^{c}	99.07^{b}	71.7^{c}
CNF-Ph1.5	0.0164^{c}	335^{d}	3.2^{d}	98.8^{b}	60.3^{d}

* Different lowercase letters in the same column show the significant difference ($P < 0.05$).

3.3. Aerogel characteristics

The results of the analysis of variances show a significant effect of different phthalimide loadings on density, porosity, specific surface area and size of pores of the resulting aerogels at a 95% confidence level. The Duncan multiple range test results (provided in Table 2) showed that at low phthalimide fraction (< 0.5%), the difference in mean density and porosity is not significant. However, at higher fraction (i.e. > 0.5%) there is a significant difference in the mentioned properties.

Concentration is one of the factors that affect the porosity and density. As the phthalimide concentration increased, the structure become denser and more compact, which results in an increase in density and a decrease in porosity (Feng, Nguyen, Fan, & Duong, 2015; Rafieian, Hosseini, Jonoobi, & Yu, 2018). In addition, Table 2 shows that the specific surface area of the modified CNF increased with the increasing phthalimide content, as the highest phthalimide specific surface area (335 m^2/g) happened when 1.5% phthalimide. It was also observed that with higher phthalimide fraction, the size of pore and the volume of pores decreased due to its high density which makes the aerogels compressed and denser (Rafieian et al., 2018; Rafieian, Jonoobi, & Yu, 2019; Rafieian, Mousavi, Yu, & Jonoobi, 2019).

3.4. ATR - IR before adsorption CO_2

Phthalimide has a hydrophilic head (-NH) and a hydrophobic end; hence, CNF could create hydrogen bonds with the fiber surface at the hydrophilic head (Marzbani, Resalati, Ghasemian, & Shakeri, 2016). The interaction between phthalimide and the CNF surfaces, as studied by ATR-IR spectrometry, are shown in Fig. 3A and B. As can be seen from Fig. 3A, the curve (a) represents the spectrum of pure phthalimide. The peaks located at 1600 cm^{-1}, 3305 cm^{-1}, and 1713 cm^{-1} are, respectively, associated with the aromatic ring, the stretching vibrations of secondary N—H amide bands, and conjugated C=O bonds (Marzbani et al., 2016). The CNF spectrum (curve b) shows a number of characteristic bands such as O—H stretching at 3346 cm^{-1}, C–H stretching at 2901 cm^{-1}, and C–O-C skeletal vibrations at 1053 cm^{-1}, while O—H and C–H bending along with C—C and C–O stretching are located at 1376, 1310, and 1253 cm^{-1}, respectively. All the peaks were identified as typical cellulose peaks (Kumar, Negi, Choudhary, & Bhardwaj, 2014). For Ph-CNF (curves c, d, and e), all spectra show the emergence of small new peaks located at approximately 1750 cm^{-1} (1740-1750 cm^{-1}), 1273 cm^{-1} (1270-1273 cm^{-1}), and 790 cm^{-1} (780-790 cm^{-1}) which are assigned to ester bonding COO-, C–N stretching, and NH_2 wagging, respectively. Thus, the existence of all the new peaks in the CNF spectrum indicate that chemical modification had occurred and that the phthalimide has grafted to the O—H functional groups on the CNF surfaces. Furthermore, Fig. 3B shows the ATR-IR spectrum of CO_2 adsorption after 8 h for modified and unmodified CNF. Up to now, no data on the ATR-IR spectra of CO_2 adsorption on phthalimide-modified CNF is available. As can be seen, the ATR-IR spectrum of unmodified CNF shows one peak, while the modified CNF shows three new peaks around 1369, 1466 and 1568 cm^{-1}. The bands at 1369 cm^{-1}, 1466 cm^{-1}, and 1568 cm^{-1} can be assigned to HCO_3-

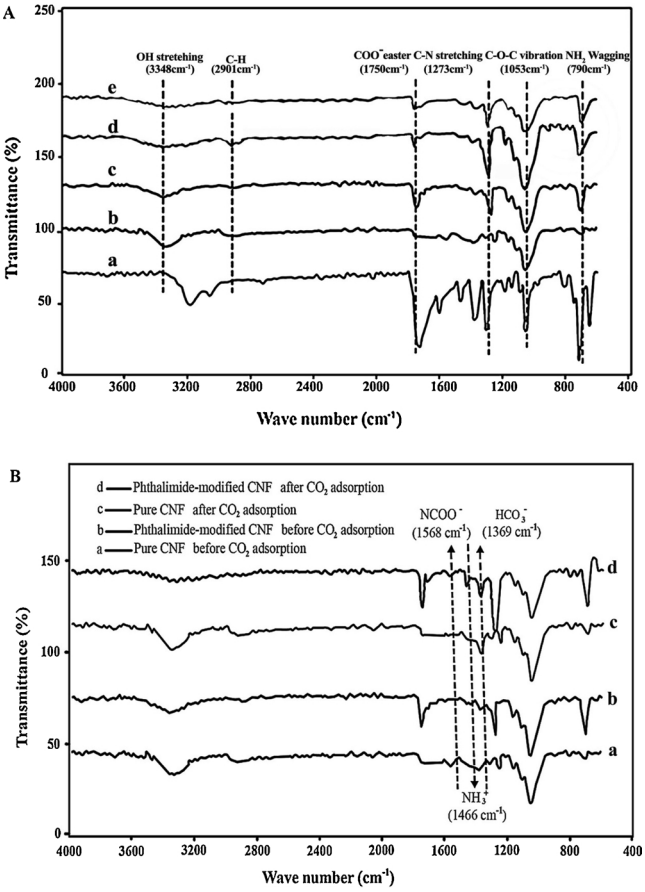

Fig. 3. A) ATR-IR spectra of (a) Ph, (b) CNF, and Ph-CNF with several ratios: (c) 1:0.5 (w/w)%, (d) 1:1 (w/w)%, and (e) 1:1.5 (w/w)%. B) Spectra of modified and unmodified CNF before and after CO_2 adsorption test.

(Gebald et al., 2011; Robinson, McCluskey, & Attalla, 2011), NH_3^+, and (N) COO- asymmetric stretching, respectively (Danon, Stair, & Weitz, 2011; Gebald et al., 2014). Regarding the CO_2 adsorption in amine solution, it is well known that CO_2 reacts with primary and secondary amines to form carbamic acid, carbamate, and bicarbonate types (Gebald et al., 2011). Based on these reactions, we know that CO_2 can react with the surface groups of unmodified and phthalimide-modified CNF (Chang, Chuang, Gray, & Soong, 2003; Gebald et al., 2011). The mechanism between CO_2, amino and carboxyl groups are detailed in Eqs. (5)–(7) below:

$$CO_2 + OH^- \rightarrow HCO_3^- \quad (5)$$

$$CO_2 + RNH_2 \rightarrow RNHCOOH \quad (6)$$

$$RNHCOOH + RNH_2 \rightarrow RNCOO^- + RNH_3^+ \quad (7)$$

3.5. CO_2 adsorption over time

Fig. 4(a) shows the outlet CO_2 concentration of CNF aerogels with and without phthalimide modification as a function of time. Interestingly, it can be seen that when phthalimide loading and measurment time increased the outlet CO_2 concentration decreased. To fully characterize the amine-based adsorbents, the CO_2 capacity rate as a function of time was also reported (Fig. 4b). As Fig. 4(b) shows, the capacity of adsorption for the pure CNF is 2.2 $mmol.g^{-1}$, this is due to the formation of a tremendous surface hydroxyl group leading to the CO_2 adsorption. In general, over time outlet CO_2 concentration decreased and CO_2 adsorption inceased meaning the effectiveness and efficiency of the resulting material is much better in the long term. When the CNF

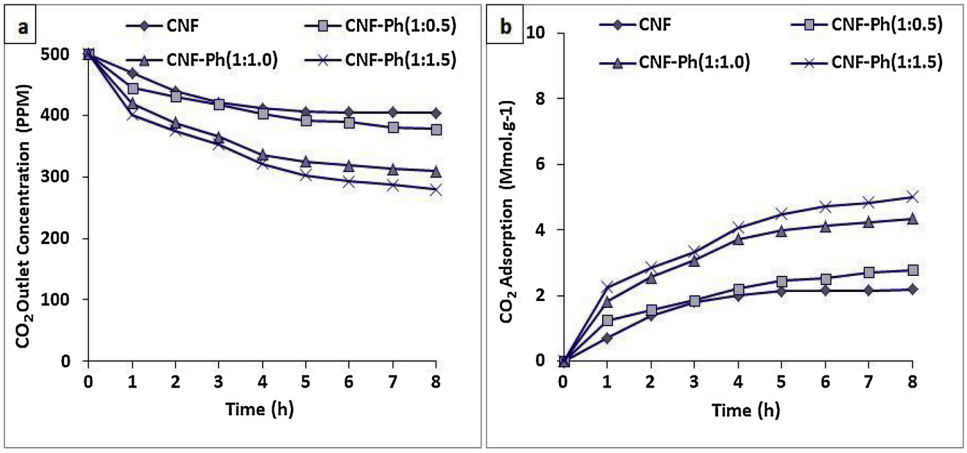

Fig. 4. Influence of different times on (a) outlet CO_2 concentration and (b) CO_2 adsorption of modified and unmodified CNF aerogel.

was modified with phthalimide the adsorption of CO_2 improved, this was reflected by the increasing adsorption capacity ranging from 2.8, 4.4, and 5.2 mmol.g^{-1} corresponding to the phthalimide dosages of 0.5, 1.0, and 1.5%, respectively. The adsorption efficiency of the modified CNF also improved by increasing phthalimide loading, with the best results associated to the 1.5% phthalimide dose. This can be related to the existence of the amino group, C═O bond on the surface-modified CNF, and the increased surface area, which all contribute to higher CO_2 adsorption. The highest CO_2 adsorption level reported in the literature is 2.3 mmol.g^{-1} by Gebald et al. (2014).

3.6. Influence of pressure and humidity

Modified and unmodified CNF aerogels with different amounts of phthalimide were investigated to examine how pressure and humidity can affect their structure and CO_2 adsorption performance. Influence of different pressure and humidity on the outlet CO_2 concentration and the CO_2 adsorption of modified and unmodified CNF aerogel are shown in Fig. 5A and B. Increasing phthalimide loading as well as measurement pressure (from 0.2 to 1 bar) under specific conditions (8 h, room temperature, and ambient humidity) caused the outlet CO_2 concentration to decrease. To fully characterize the amine-based adsorbents, the CO_2 adsorption rate as a function of pressure were reported (Fig. 5A (a, b)). The results clearly indicate that the CO_2 adsorption improved significantly by increasing pressure from 4 to 7.1 mmol.g^{-1}. This is because CO_2 has a large quadrupole moment, which is the reason for its strong interaction with the functional groups present on the surface at high pressure (Dassanayake, Gunathilake, Dassanayake, Abidi, & Jaroniec, 2017; Salehi & Anbia, 2017). In addition, aerogels with different phthalimide loadings were investigated to study how humidity level affects the structure and CO_2 adsorption performance of modified and unmodified CNF. Fig. 5B (a) shows the outlet concentration of CO_2 for modified and unmodified CNF aerogels at different humidities ranging from 25 to 95% for the same time (8 h), pressure (1 bar), and room temperature. As can be seen in the figure, when phthalimide loading and humidity increases the outlet CO_2 concentration decreases. CO_2 adsorption rate as a function of relative humidity (RH) were also reported (Fig. 5B (b)). The results can be used to explain why high humidity levels lead to greater CO_2 adsorption for modified and unmodified CNF aerogels. CO_2 adsorption increased when the phthalimide loading increased from 0.5 to 1.5% in the modified CNF aerogels, the highest level of adsorbed CO_2 was reached at RH 95% and a phthalimide of 1.5% (5.5 mmol.g^{-1}). This is probably due to the amines existing in the phthalimide, which caused CO_2 adsorption under the catalytic effect of RH, high pressure at ambient temperature (Choi et al., 2011). Since polar water molecules and non-polar CO_2 molecules easily dissolve in water, increasing RH leads to improved CO_2 adsorption.

3.7. Influence of temperature and flow rate

In addition to humidity, temperature and flow rate are other critical environmental factors that can affect CO_2 adsorption. Hence, the effects of temperature and flow rate on CO_2 adsorption were investigated. The influences of different temperature and flow rate on outlet CO_2 concentration and the CO_2 adsorption of modified and unmodified CNF aerogel are shown in (Fig. 6A and B). For this purpose, practical atmospheric temperatures from a range of 25 to 85 °C were chosen to study the effects of temperature on the CO_2 adsorption of the filters. Fig. 6A (a) shows the outlet CO_2 concentration for modified and unmodified CNF aerogels in response to different temperatures for the same time (8 h) and pressure (1 bar). As can be seen, the outlet CO_2 concentration decreased. Fig. 6A (b) indicates the results of temperature change on the adsorption of CO_2. It can be seen that as the temperature and phthalimide loading increase from 25 to 85 °C and 0.5 to 1.5%, respectively, the adsorption of CO_2 increased from 4.1 to 6.5 mmol.g^{-1}. This phenomenon could be explained by the fact that the amino groups of phthalimide accelerated CO_2 adsorption. Overall, the temperature was found to have a greater on influence the adsorption of the CO_2 than flow rate, especially when the pressure was high, since increasing temperature and pressure promotes the kinetic energy of CO_2 molecules resulting in an increase in the CO_2 adsorption (Dassanayake et al., 2017; Guan, Liu, Li, Wang, & Zhao, 2018).

In addition, the effects of different airflow rates on the structure, CO_2 adsorption, and performance of modified and unmodified CNF aerogels with different amounts of phthalimide were also studied. Fig. 6B (a) shows the amount of the outlet CO_2concentration for CNF aerogels with and without phthalimide modification as a function of flow rate. As can be seen, increasing the amount of phthalimide and flow rate from 0.2 to 0.8 l/min under specific conditions of time (8 h), pressure (1 bar) at room temperature, and ambient humidity caused the outlet CO_2 concentration to decrease. To better understand the characteristics of the amine-based adsorbents, the CO_2 adsorption rate as a function of flow rate was also reported in Fig. 6B (b). It was observed that increasing the flow rate in the modified and unmodified CNF at 0.5% phthalimide loading had no significant effect on the adsorption of CO_2, but it increased the CO_2 adsorption efficiency when the amount of phthalimide rose. This can be explained by the fact that when the flow rate increased the interfacial area between the CO_2 molecules and amino groups also increased. The enhanced CO_2 molecules transfer rate and improved CO_2 adsorption efficiency results are in agreement with a recent study (Rahmandoost, Roozbehani, & Maddahi, 2014).

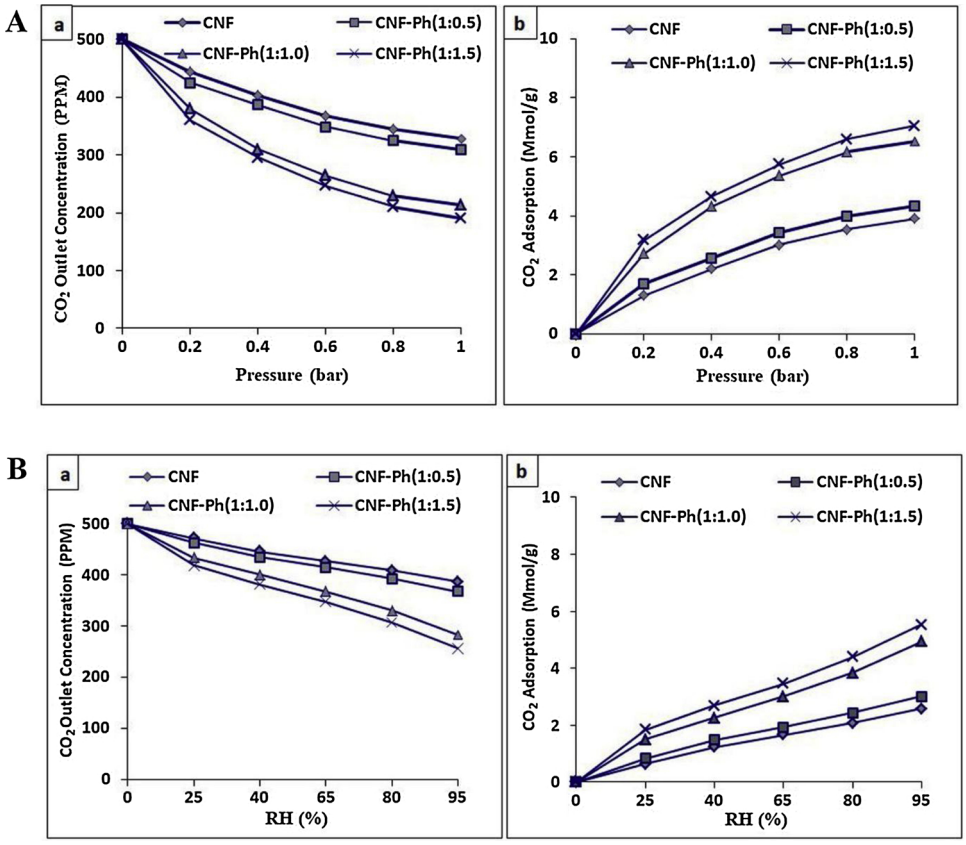

Fig. 5. A) Influence of different pressures and **B)** Influence of different humidities on (a) outlet CO_2 concentration and (b) the CO_2 adsorption of modified and unmodified CNF aerogel.

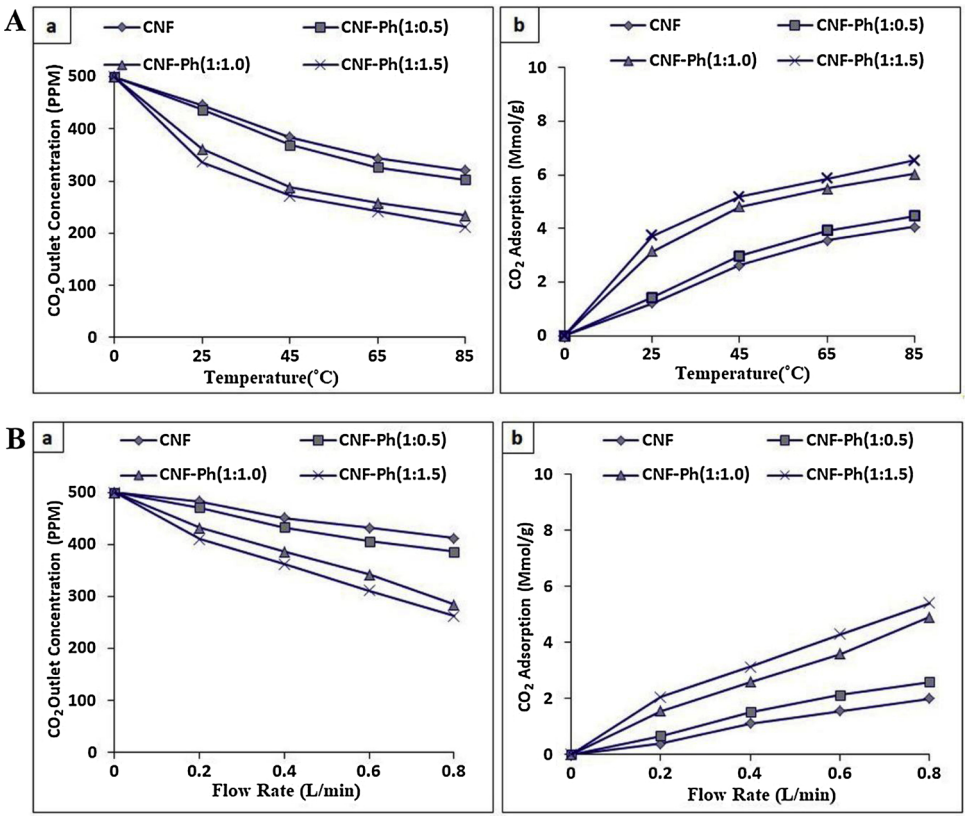

Fig. 6. A) Influence of different temperatures and B) Influence of different flow rates on (a) outlet CO_2 concentration and (b) the CO_2 adsorption of modified and unmodified CNF aerogel.

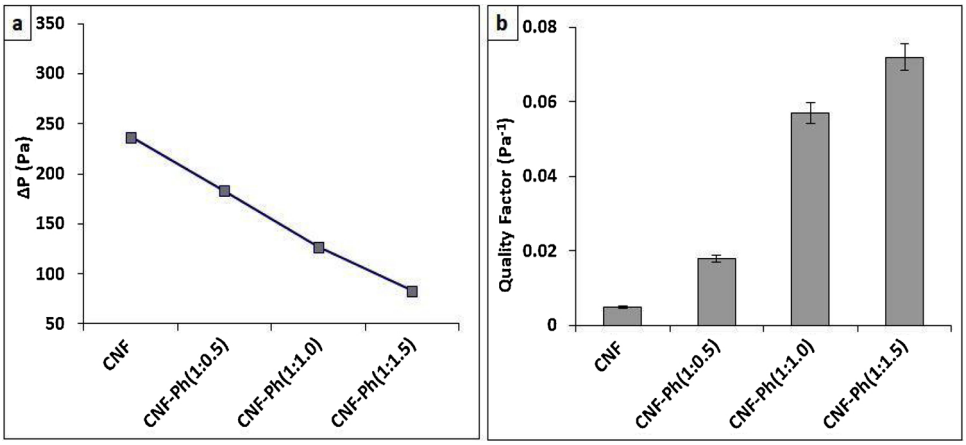

Fig. 7. (a) Pressure drops and (b) quality factors of modified and unmodified CNF.

3.8. Air flow permeability (pressure drop, ΔP) and quality factor (QF) measurement

In addition to the adsorption of CO_2, the pressure drop or airflow resistance of an air filter is another parameter related to filtration performance. It should be noted that air filtration efficiency should also take into account the airflow resistance (or pressure drop) since it is related to the filter's energy consumption. High filtration efficiency possesses a pressure drop of less than 325 Pa at a standard air face velocity of 5 cm/s (DOE standard, 2005). Fig. 7(a) shows a quantitative study on the effects of airflow resistance on the unmodified and modified CNF with phthalimide ratios of 1:0.5, 1:1, and 1:1.5%. As the figure shows, the pressure drop generally decreases linearly, which might be related to its surface area, size of pores, fiber diameter and pore structure. It has already been suggested that a good air filter should have a high QF value, in other words, a good air filter can achieve high adsorption efficiency with a low pressure drop or air resistance (Souzandeh, Johnson, Wang, Bhamidipaty, & Zhong, 2016). A comparison of QF values among different types of air filtering with modified and unmodified CNF is shown in Fig. 7(b). This comparison demonstrates that the optimized CNF modified with 1.5% phthalimide has the highest QF value ($0.072\ Pa^{-1}$) among these different types, implying that the CNF with 1.5% phthalimide provides the best filtration performance.

3.9. Influence of humidity, temperature, pressure, and flow rate on the airflow resistance (ΔP)

It is proven that environmental conditions, such as humidity, temperature, pressure, and flow rate, can noticeably change the pores structure of the filter, and subsequently considerably affect the air flow inside the filter (Souzandeh, Molki et al., 2017; Souzandeh, Scudiero, Wang, & Zhong, 2017). Therefore, in addition to the adsorption efficiency, air flow resistance (also known as pressure drop *(ΔP)*) for the modified and unmodified CNF aerogels were studied at different humidity, pressures, flow rate levels, and higher temperatures (Fig. 8). As can be seen from Fig. 8(a), the pressure drop slightly increased when temperatures of the modified and unmodified samples increased. The unmodified sample possessed a pressure drop ranging from 168 to 178 Pa, while the CNF samples modified with phthalimide amounts of 0.5, 1, and 1.5% exhibited an air flow resistance ranging from 166 to 176, 164 to 173, and 163 to 170 Pa, respectively, when the temperature increased from 25 to 85 °C. Additionally, the effects of humidity relative to the pressure drop for the modified and unmodified samples are shown in Fig. 8(b). As can be seen, the air flow resistance increased for unmodified CNF from 144 to 155 Pa when RH increased from 25 to 95%. In contrast, the CNF samples modified with phthalimide loadings of 0.5, 1, and 1.5% showed an air flow resistance ranging from 143 to 151, 142 to 150, and 140 to 148 Pa, respectively, when the RH increased from 25 to 95%. The trend of decreasing air flow for the modified samples as compared to the unmodified samples may be due to the solubility of some of the phthalimide in high moisture content (Souzandeh, Molki et al., 2017; Souzandeh, Scudiero et al., 2017). Nevertheless, the results indicate that moisture does not have a significant effect on the structure of the samples. As shown in Fig. 8(c), the pressure drop increased only slightly from 148 to 157 Pa for unmodified CNF and from 146 to 154, 145 to 152, and 144 to 150 for CNF modified with phthalimide loadings of 0.5, 1, and 1.5%, respectively, when the pressure increased from 0.2 to 1 bar. This increase in flow rate could also be due to greater thickness since the increased thickness resulted in an increase in pressure drop. In fact, thickness is an effective parameter on the pressure drop of an air filter (Zhang et al., 2016). The effect of flow rate on air flow resistance of the modified and unmodified CNF is shown in Fig. 8(d). This increase could be due to changes in the air stream pathway as it passes through the thickness of the filter (Souzandeh, Molki et al., 2017; Souzandeh, Scudiero et al., 2017). In summary, for all samples the pressure drop slightly increased under the above conditions, but this pressure drop was below the DOE (Department of Energy) standard. In other words, the above conditions do not have a considerable effect on the fiber diameter and pores structure.

4. Conclusions

This study showed that phthalimide-modified CNF represents a promising green nanomaterial with great potential for CO_2 adsorption from the atmosphere. The following conclusions can be drawn from the results of this study. The ATR-IR analysis revealed three new peaks of COO^-, C–N, and NH_2, which confirm the success of grafting phthalimide on CNF. BET analysis revealed an increase in surface area and a decrease in size of pores after the modification of CNF. The XPS results showed that the peak at 399.39 eV can be attributed to the existence of free amino groups (-NH_2) in the phthalimide. In total, the nitrogen content increased with the increase in phthalimide loading. However, the thermal stability of the modified CNF decreased, this is probably due to the replacement of OH groups in the CNF by NH_2 groups in the phthalimide. In general, increasing the amount of phthalimide (1.5%) in the modified CNF significantly increased the adsorption of CO_2. This phenomenon is probably due to the incorporation of amine groups on the surface of the modified CNF, and also the increase in the surface area as a result of the addition of phthalimide. Temperature, humidity, pressure and flow rate have a strong influence on CO_2 adsorption without changing the CNF's structure. Increasing the temperature, humidity, pressure, and flow rate caused an increase in the pressure drop, especially in unmodified CNF samples, although the increase was less

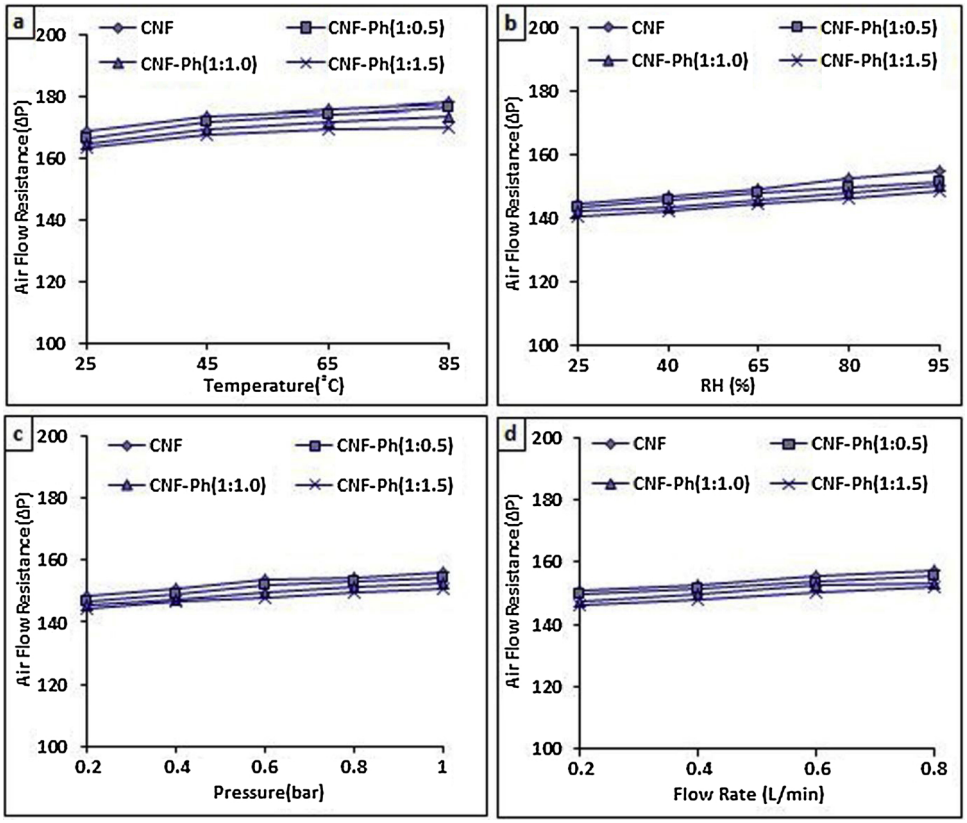

Fig. 8. Effects of (a) temperature, (b) humidity, (c) pressure, and (d) flow rate on the air flow resistance (ΔP) of modified and unmodified CNF aerogels.

than the DOE standard (325 Pa). The modified CNF is able to decrease the air flow resistance (pressure drop) while also increase the Quality Factor, which are the most crucial factors for practical applications.

Acknowledgment

The authors thank the University of Tehran, Iran and the Iran Nanotechnology Initiative Council (INIC), Iran. Moreover, many thanks to the Department of the Built Environment of the Eindhoven University of Technology for funding this research; and the Bio4Energy Program, Sweden for providing financial support during this research.

References

Aaron, D., & Tsouris, C. (2005). Separation of CO_2 from flue gas: A review. *Separation Science and Technology, 40*(1-3), 321–348.

Adiletta, J.G. Fibrous nonwoven web. US Patent5, 954, 962, 21 Sep1999.

Ansaloni, L., Salas-Gay, J., Ligi, S., & Baschetti, M. G. (2017). Nanocellulose-based membranes for CO_2 capture. *Journal of Membrane Science, 522*, 216–225.

Böcking, T., James, M., Coster, H. G., Chilcott, T. C., & Barrow, K. D. (2004). Structural characterization of organic multilayers on silicon (111) formed by immobilization of molecular films on functionalized Si− C linked monolayers. *Langmuir, 20*(21), 9227–9235.

Chaabouni, O., & Boufi, S. (2017). Cellulose nanofibrils/polyvinyl acetate nanocomposite adhesives with improved mechanical properties. *Carbohydrate Polymers, 156*, 64–70.

Chang, A. C., Chuang, S. S., Gray, M., & Soong, Y. (2003). In-situ infrared study of CO_2 adsorption on SBA-15 grafted with γ-(aminopropyl) triethoxysilane. *Energy & Fuels, 17*(2), 468–473.

Chenite, A., & Selmani, A. (1994). Cr/phthalimide system: XPS study of interfacial reactions. *Surface Science, 301*(1–3), 197–202.

Choi, S., Drese, J. H., Eisenberger, P. M., & Jones, C. W. (2011). Application of amine-tethered solid sorbents for direct CO_2 capture from the ambient air. *Environmental Science & Technology, 45*(6), 2420–2442.

Danon, A., Stair, P. C., & Weitz, E. (2011). FTIR study of CO_2 adsorption on amine-grafted SBA-15: Elucidation of adsorbed species. *The Journal of Physical Chemistry C, 115*(23), 11540–11549.

Darunte, L. A., Walton, K. S., Sholl, D. S., & Jones, C. W. (2016). CO_2 capture via adsorption in amine-functionalized sorbents. *Current Opinion in Chemical Engineering, 12*, 82–90.

Dassanayake, R. S., Gunathilake, C., Jackson, T., Jaroniec, M., & Abidi, N. (2016). Preparation and adsorption properties of aerocellulose-derived activated carbon monoliths. *Cellulose, 23*(2), 1363–1374.

Dassanayake, R. S., Gunathilake, C., Dassanayake, A. C., Abidi, N., & Jaroniec, M. (2017). Amidoxime-functionalized nanocrystalline cellulose–mesoporous silica composites for carbon dioxide sorption at ambient and elevated temperatures. *Journal of Materials Chemistry A, 5*(16), 7462–7473.

Dawson, R., Adams, D. J., & Cooper, A. I. (2011). Chemical tuning of CO_2 sorption in robust nanoporous organic polymers. *Chemical Science, 2*(6), 1173–1177.

DOE, U.S.D.E. DOE technical standard (2005). *Specification for HEPA filters used by DOE contractor.* Washington, D.C..

Fan, X., Zhang, L., Zhang, G., Shu, Z., & Shi, J. (2013). Chitosan derived nitrogen-doped microporous carbons for high performance CO_2 capture. *Carbon, 61*.

Feng, J., Nguyen, S. T., Fan, Z., & Duong, H. M. (2015). Advanced fabrication and oil absorption properties of super-hydrophobic recycled cellulose aerogels. *Chemical Engineering Journal, 270*, 168–175.

Gao, K., Shao, Z., Li, J., Wang, X., Peng, X., Wang, W., ... Wang, F. (2013). Cellulose nanofiber–graphene all solid-state flexible supercapacitors. *Journal of Materials Chemistry A, 1*(1), 63–67.

Gebald, C., Wurzbacher, J. A., Tingaut, P., Zimmermann, T., & Steinfeld, A. (2011). Amine-based nanofibrillated cellulose as adsorbent for CO_2 capture from air. *Environmental Science & Technology, 45*(20), 9101–9108.

Gebald, C., Wurzbacher, J. A., Borgschulte, A., Zimmermann, T., & Steinfeld, A. (2014). Single-component and binary CO_2 and H_2O adsorption of amine-functionalized cellulose. *Environmental Science & Technology, 48*(4), 2497–2504.

Guan, C., Liu, S., Li, C., Wang, Y., & Zhao, Y. (2018). The temperature effect on the methane and CO_2 adsorption capacities of Illinois coal. *Fuel, 211*, 241–250.

Hao, G. P., Li, W. C., & Lu, A. H. (2011). Novel porous solids for carbon dioxide capture. *Journal of Materials Chemistry, 21*(18), 6447–6451.

Hornbostel, M. D., Bao, J., Krishnan, G., Nagar, A., Jayaweera, I., Kobayashi, T., ... Dubois, L. (2013). Characteristics of an advanced carbon sorbent for CO_2 capture. *Carbon, 56*, 77–85.

Hung, C. H., & Leung, W. W. F. (2011). Filtration of nano-aerosol using nanofiber filter under low Peclet number and transitional flow regime. *Separation and purification technology, 79*(1), 34–42.

Jonoobi, M., Ashori, A., & Siracusa, V. (2019). Characterization and properties of polyethersulfone/modified cellulose nanocrystals nanocomposite membranes. *Polymer Testing, 76*, 333–339.

Jonoobi, M., Harun, J., Mathew, A. P., & Oksman, K. (2010). Mechanical properties of cellulose nanofiber (CNF) reinforced polylactic acid (PLA) prepared by twin screw extrusion. *Composites Science and Technology, 70*(12), 1742–1747.

Khanjanzadeh, H., Behrooz, R., Bahramifar, N., Pinkl, S., & Gindl-Altmutter, W. (2019). Application of surface chemical functionalized cellulose nanocrystals to improve the performance of UF adhesives used in wood based composites-MDF type. *Carbohydrate*

Polymers, 206, 11–20.
Kumar, A., Negi, Y. S., Choudhary, V., & Bhardwaj, N. K. (2014). Characterization of cellulose nanocrystals produced by acid-hydrolysis from sugarcane bagasse as agro-waste. *Journal of Materials Physics and Chemistry, 2*(1), 1–8.
Liu, X., Souzandeh, H., Zheng, Y., Xie, Y., Zhong, W. H., & Wang, C. (2017). Soy protein isolate/bacterial cellulose composite membranes for high efficiency particulate air filtration. *Composites Science and Technology, 138*, 124–133.
Lu, J., Askeland, P., & Drzal, L. T. (2008). Surface modification of microfibrillated cellulose for epoxy composite applications. *Polymer, 49*(5), 1285–1296.
Ma, H., Hsiao, B. S., & Chu, B. (2011). Thin-film nanofibrous composite membranes containing cellulose or chitin barrier layers fabricated by ionic liquids. *Polymer, 52*(12), 2594–2599.
Mahfoudhi, N., & Boufi, S. (2017). Nanocellulose as a novel nanostructured adsorbent for environmental remediation: A review. *Cellulose, 24*(3), 1171–1197.
Marzbani, P., Resalati, H., Ghasemian, A., & Shakeri, A. (2016). Surface modification of talc particles with phthalimide: Study of composite structure and consequences on physical, mechanical, and optical properties of deinked pulp. *BioResources, 11*(4), 8720–8738.
Molina, C. T., & Bouallou, C. (2016). Carbon dioxide absorption by ammonia intensified with membrane contactors. *Clean Technologies and Environmental Policy, 18*(7), 2133–2146.
Olmedo, C. G., Aragón, E. Q., Garcia, J., Torrent, L. M. P., & Ramón, C. F. (2008). *Study of porosity and permeability of air filter material in respiratory protection filters. International Multidisciplinary Scientific GeoConference: SGEM: Surveying Geology & Mining Ecology Management, Vol. 1*, 231.
Rafieian, F., Hosseini, M., Jonoobi, M., & Yu, Q. (2018). Development of hydrophobic nanocellulose-based aerogel via chemical vapor deposition for oil separation for water treatment. *Cellulose, 25*(8), 4695–4710.
Rafieian, F., Jonoobi, M., & Yu, Q. (2019). A novel nanocomposite membrane containing modified cellulose nanocrystals for copper ion removal and dye adsorption from water. *Cellulose, 26*, 3359–3373.
Rafieian, F., Mousavi, M., Yu, Q., & Jonoobi, M. (2019). Amine functionalization of microcrystalline cellulose assisted by (3-chloropropyl) triethoxysilane. *International Journal of Biological Macromolecules, 130*, 280–287.
Rahmandoost, E., Roozbehani, B., & Maddahi, M. H. (2014). Experimental studies of CO_2 capturing from the flue gases. *Iranian Journal of Oil & Gas Science and Technology, 3*(4), 1–15.
Robinson, K., McCluskey, A., & Attalla, M. I. (2011). An FTIR spectroscopic study on the effect of molecular structural variations on the CO_2 absorption characteristics of heterocyclic amines. *ChemPhysChem, 12*(6), 1088–1099.
Salehi, S., & Anbia, M. (2017). High CO_2 adsorption capacity and CO_2/CH_4 selectivity by nanocomposites of MOF-199. *Energy & Fuels, 31*(5), 5376–5384.
Sehaqui, H., Gálvez, M. E., Becatinni, V., cheng Ng, Y., Steinfeld, A., Zimmermann, T., ... Tingaut, P. (2015). Fast and reversible direct CO_2 capture from air onto all-polymer nanofibrillated cellulose- polyethylenimine foams. *Environmental Science & Technology, 49*(5), 3167–3174.
Sepahvand, S., Jonoobi, M., Ashori, A., Gauvin, F., Brouwers, H. J. H., & Yu, Q. (2019). Surface modification of cellulose nanofiber aerogels using phthalimide. *Polymer Composites*. https://doi.org/10.1002/pc.25362.
Shou, D., Fan, J., Ye, L., Zhang, H., Qian, X., & Zhang, Z. (2015). Inverse problem of air filtration of nanoparticles: Optimal quality factors of fibrous filters. *Journal of Nanomaterials, 16*(1), 351.
Song, J., & Peng, P. A. (2009). Surface characterization of aerosol particles in Guangzhou, China: A study by XPS. *Aerosol Science and Technology, 43*(12), 1230–1242.
Souzandeh, H., Johnson, K. S., Wang, Y., Bhamidipaty, K., & Zhong, W. H. (2016). Soy-protein-based nanofabrics for highly efficient and multifunctional air filtration. *ACS Applied Materials & Interfaces, 8*(31), 20023–20031.
Souzandeh, H., Molki, B., Zheng, M., Beyenal, H., Scudiero, L., Wang, Y., & Zhong, W. H. (2017). Cross-linked protein nanofilter with antibacterial properties for multi-functional air filtration. *ACS Applied Materials & Interfaces, 9*(27), 22846–22855.
Souzandeh, H., Scudiero, L., Wang, Y., & Zhong, W. H. (2017). A disposable multi-functional air filter: Paper towel/protein nanofibers with gradient porous structures for capturing pollutants of broad species and sizes. *ACS Sustainable Chemistry & Engineering, 5*(7), 6209–6217.
Stein, A., Wang, Z., & Fierke, M. A. (2009). Functionalization of porous carbon materials with designed pore architecture. *Advanced Materials, 21*(3), 265–293.
Sung, S., & Suh, M. P. (2014). Highly efficient carbon dioxide capture with a porous organic polymer impregnated with polyethylenimine. *Journal of Materials Chemistry A, 2*(33), 13245–13249.
Tingaut, P., Hauert, R., & Zimmermann, T. (2011). Highly efficient and straightforward functionalization of cellulose films with thiol-ene click chemistry. *Journal of Materials Chemistry, 21*(40), 16066–16076.
Yoon, K., Hsiao, B. S., & Chu, B. (2008). Functional nanofibers for environmental applications. *Journal of Materials Chemistry, 18*(44), 5326–5334.
Zhang, R., Liu, C., Hsu, P. C., Zhang, C., Liu, N., Zhang, J., ... Cui, Y. (2016). Nanofiber air filters with high-temperature stability for efficient $PM_{2.5}$ removals from the pollution sources. *Nano Letters, 16*(6), 3642–3649.